J. Electroanal. Chem., 134 (1982) 251–272
Elsevier Sequoia S.A., Lausanne—Printed in The Netherlands

THE ELECTROCHEMICAL BEHAVIOUR OF COBALT IN ALKALINE SOLUTIONS

PART I. THE POTENTIODYNAMIC RESPONSE IN THE POTENTIAL REGION OF THE Co/CoO COUPLE

H. GOMEZ MEIER *, J.R. VILCHE and A.J. ARVIA **

Instituto de Investigaciones Fisicoquímicas Teóricas y Aplicadas, (INIFTA), División Electroquímica. Sucursal 4—Casilla de Correo 16, (1900) La Plata (Argentina)

(Received 15th September 1981; in revised form 2nd November 1981)

ABSTRACT

The potentiodynamic response of cobalt in KOH solutions ($10^{-2} M \leqslant c \leqslant 2.5 M$) in the potential range of the thermodynamic stability of the Co(II) species reveals two limiting electrochemical behaviours. One of them corresponds to the first potentiodynamic scan and the other is associated with the stabilized E/I profile resulting after a prolonged potential scanning. The former is related to the large contribution of the metal electrodissolution process. The second is explained in terms of reactions taking place at the sandwich-type structured interface. Ageing effects of Co(II) surface species are also considered in the interpretation of results.

INTRODUCTION

The electrochemical behaviour of the iron group metals in alkaline electrolytes has long been studied. However, the number of contributions on iron and nickel appearing in the literature exceeds by far those related to cobalt [1,2]. This is probably because of the apparent irreversibility of the electrochemical reactions of cobalt which limit its application in electrochemical energy storage. However, small amounts of cobalt improve the efficiency of nickel–iron and nickel–cadmium cells [3] producing an increase both in the conductivity of the electrode material and in the charging efficiency [4]: The electrocatalytic properties of spinel-type cobalt oxides in alkaline solutions, as well as their chemical and electrochemical stability have been recently analysed [5].

Various cobalt oxides and hydroxides can be formed on the metal during anodization in alkaline solutions [6–10], but at present there is considerable dis-

* Present address: Instituto de Química, Universidad Católica de Valparaíso, Chile.
** To whom correspondence should be addressed.

0022-0728/82/0000–0000/$02.75

agreement about the most likely structure of the species produced at different potentials. Some authors found three different electrochemical oxidation stages of cobalt which were assigned, respectively, to the formation of CoO, Co_2O_3 and Co_3O_4 [7], while others reported only two stages which were related to $Co(OH)_2$ and CoOOH [11]. More recently, the passivity of cobalt in buffer borate solutions in the pH range between 7 and 11 [12–17] was related to a film which is made up of different layers of hydrated cobalt oxides. The primary layer of about 2.5 nm thickness corresponds to hydrated CoO, the second layer is made of hydrated Co_3O_4 whose thickness is potential dependent and varied between 1.5 and 5.0 nm. Finally, the third layer which is also potential dependent has a thickness between 1.5 and 3.5 nm. Mössbauer spectroscopy made *in situ* on a cobalt electrode in a buffered borate solution at pH 8.5 [18–20] revealed the formation of $Co(OH)_2$ when the applied potential is -0.1 V (vs. SCE). In the 0.2 V–0.5 V range the main species at the surface would be β-CoOOH and in the transpassive region (> 0.8 V) the formation of CoO_2 probably takes place.

The application of cyclic voltammetry, rotating disc and ring-disc techniques to cobalt electrodes in 0.2–8 *M* KOH indicate the formation of Co(II) soluble species during the metal electrodissolution [21] and the growth of a $Co(OH)_2$ layer which later electro-oxidizes to Co_3O_4 and CoOOH [22–24]. The use of potentiostatic techniques combined with interference microscopy [25] applied to cobalt in 1–8 *M* KOH shows three electro-oxidation reactions in the -1 to 0 V range. At low potentials $Co(OH)_2$ is apparently formed through a nucleation and growth mechanism, while in the -0.6 V to -0.5 V range the growth of an epitaxial CoO layer in the saturated solution takes place. In the intermediate potential range both processes occur simultaneously.

The aim of the present work is to investigate the cobalt/alkaline solution interface through the use of complex potentiodynamic perturbation techniques to determine the existence of ageing effects related to the film formation processes. Owing to the fact that cobalt can be oxidized to different states, the potential range was limited to that corresponding to the thermodynamic stability of Co(II) species. Finally, the electrochemical behaviour of cobalt in alkaline solutions, within the Co/Co(II) electrode potential range, is correlated to the behaviour expected for sandwich-type electrochemical interfaces already described for various metals covered by different metal oxides and hydroxides [26–30].

EXPERIMENTAL

The experimental setup was the same as described in previous publications related to the electrochemical behaviour of nickel electrodes in aqueous solutions [31–33]. "Specpure" cobalt (Johnson Matthey Chemicals) in the form of either fixed wires (0.5 mm diameter, 0.25 cm^2 apparent area) or rotating disc (0.070 cm^2 apparent area) supported with PTFE holders was used as working electrode. The counter electrode was a large area Pt sheet previously cleaned with the usual procedures.

The following electrolytic solutions were employed: 1 *M* KOH (solution A); 0.1 *M*

KOH (solution B); 0.1 *M* KOH + 0.3 *M* K_2SO_4 (solution C); 0.01 *M* KOH + 0.33 *M* K_2SO_4 (solution D); 2.5 *M* KOH (solution E). They were prepared from thrice-distilled water and analytical grade (p.a. Merck) reagents.

Potentials were measured vs. a Hg/HgO reference electrode prepared by using the same KOH solution as employed in the corresponding experiments (Hg/HgO/KOH(eg)/H_2(g), Pt; $E^0 = 0.926$ V). The correction for the liquid junction potential was 4 mV for solution C and 17 mV for solution D.

Experiments were made under N_2 gas saturation at 25°C using the following potential perturbation programs:

(1) Triangular potential scans either single (STPS) or repetitive (RTPS) between preset cathodic ($E_{s,c}$) and anodic ($E_{s,a}$) switching potentials.

(2) A RTPS including an intermediate—either potentiostatic or open-circuit—ageing.

(3) A RTPS including an intermediate potentiodynamic ageing.

The complex potential/time perturbations (2) and (3) are depicted in the corresponding figures.

RESULTS

E/I profiles run with RTPS

The potentiodynamic *E/I* profiles run with the polycrystalline Co/1 *M* KOH interface under RTPS in a potential range exceeding that of the thermodynamic stability of bulk water involve a multiplicity of anodic and cathodic current peaks (Fig. 1a, b), which depend both on the potential sweep rate (v) as well as on the number of potential sweeps (N), but the multiplicity is practically independent of the rate of stirring (ω). A reasonably stable *E/I* profile between $E_{s,c} = -1.30$ V and $E_{s,a} = 0.65$ V is attained after 60 min potential cycling at 0.03 V s^{-1}.

Initially, the total anodic charge ($Q_{a,T}$) is larger than the total cathodic charge ($Q_{c,T}$), but as the stable profile is attained the $Q_{a,T}/Q_{c,T}$ ratio approaches unity. During the positive-going potential scan a wide and complex anodic current peak (peak II) is recorded at ca. −0.55 V which is preceded by a hump at ca. −0.8 V (peak I). A complex anodic contour is observed in the −0.2 V–0.5 V potential range, where a small hump at 0.05 V (peak III) and two peaks, one at 0.15 V (peak IV) and another at 0.35 V (peak V), are distinguished. At ca. 0.6 V the contribution of the O_2 evolution current is also depicted. During successive cycles the anodic charge decreases very rapidly in the −1.0 V to −0.3 V range or thereabouts, and the peak potentials move towards more negative potential values. Practically no anodic charge decrease is observed in the 0 V–0.5 V range, but instead, a drastic change in the peak multiplicity occurs during cycling. Thus, while peak V decreases, peak IV becomes sharper and located towards more negative potentials. Simultaneously, the anodic current in the potential range of the O_2 evolution reaction slightly increases.

During the negative-going potential scan two broad but relatively small cathodic current peaks, one at 0.2 V (peak VI) and another at −0.7 V (peak VII) respectively,

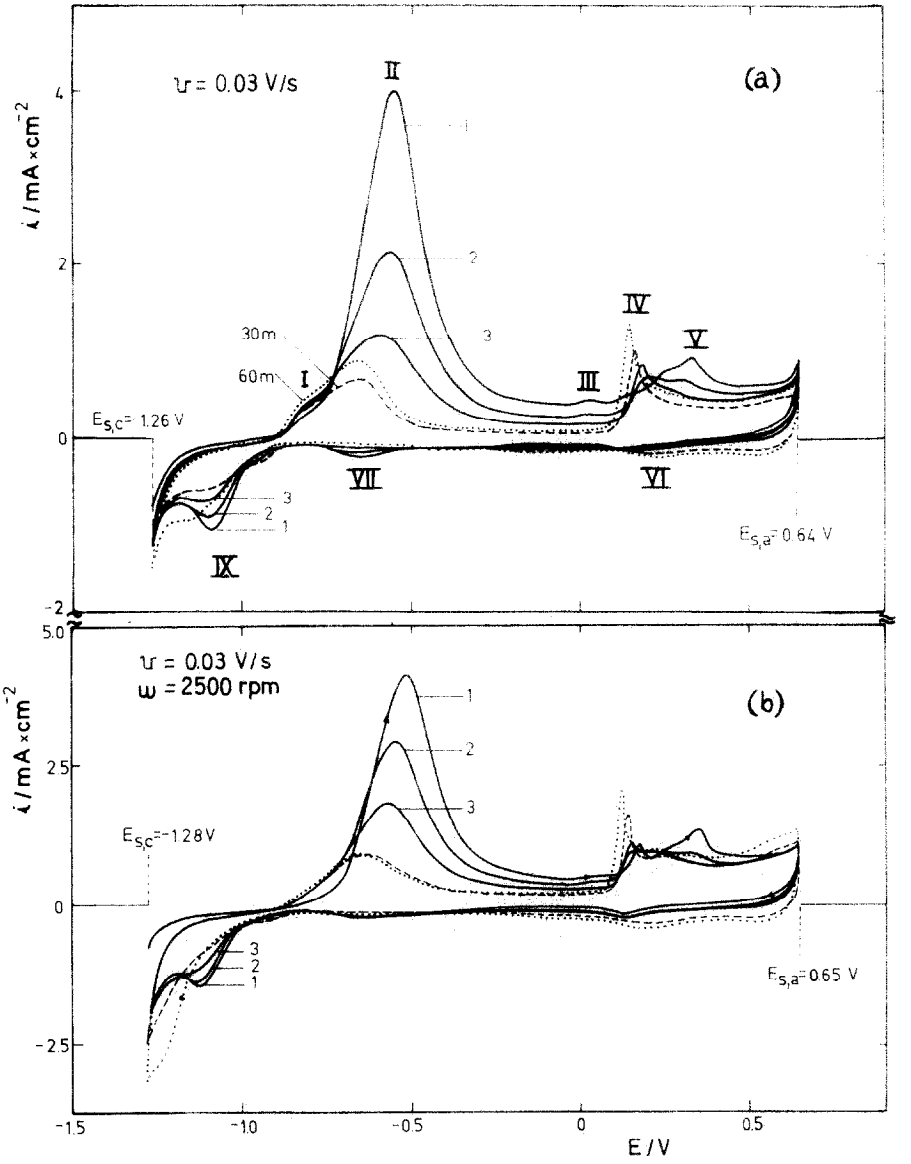

Fig. 1. Potentiodynamic E/I profiles run with RTPS at $v = 0.03$ V s^{-1} in solution A. The first, second and third successive cycles are indicated. The dashed and dotted lines correspond to the profiles after 30 min and 60 min potential cycling respectively. (a) $\omega = 0$; (b) $\omega = 2500$ rpm.

are observed. Finally, a net cathodic current peak appears at ca. -1.1 V (peak IX) which overlaps in part the H_2 evolution current contribution. During cycling peak IX tends to disappear, while after prolonged cycling a net hump at ca. -1.2 V is recorded. Moreover, after the RTPS, the cathodic charge contribution in the

−0.2 V–0.5 V range gradually increases to attain the value corresponding to the stabilized E/I profile.

A more detailed description of the voltammogram can be made by confining the range of the perturbing potential scans between $E_{s,c} = -1.18$ V and $E_{s,a} = -0.2$ V (Fig. 2). The E/I profile is related to the electrochemical reactions involving the initial stages of the metal electrodissolution and passivation. The RTPS E/I displays show that peak II practically disappears after prolonged cycling. Conversely, peak I at −0.74 V remains practically unaltered during cycling. These changes indicate that the RTPS is associated with the electrode passivation. Simultaneously, the corresponding cathodic E/I profiles show a remarkable decrease of peak IX and the resolution of a sharp cathodic current peak at −1.0 V (peak VIII). The height of the latter apparently increases, at least in part, at the expense of peak IX. Peaks IX and VIII are responsible for the isopotential at −1.02 V. However, the progressive

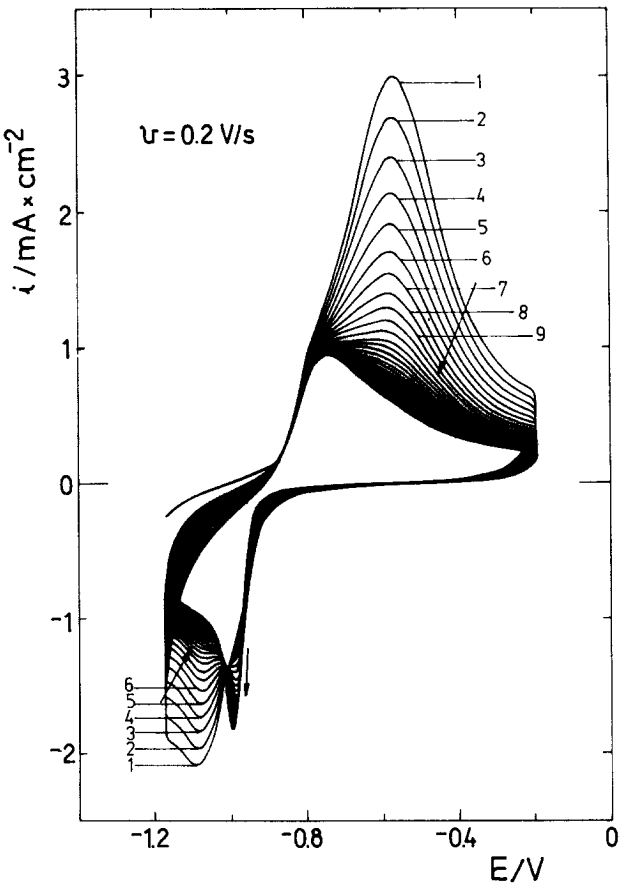

Fig. 2. E/I profiles run under RTPS from $E_{s,c} = -1.18$ V to $E_{s,a} = -0.2$ V at $v = 0.2$ V s^{-1}. The arrows indicate changes in the profile during the successive potential cycles. Solution A.

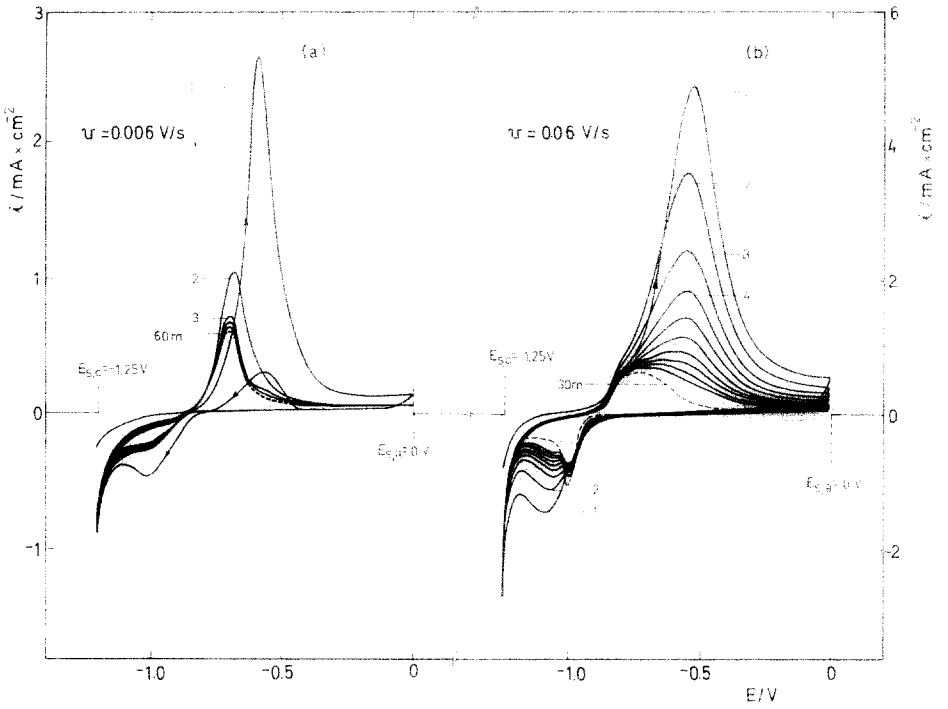

Fig. 3. Potentiodynamic E/I displays recorded with RTPS between $E_{s,c} = -1.25$ V and $E_{s,a} = 0$ V in solution A. (a) $v = 0.006$ V s^{-1}; (b) $v = 0.06$ V s^{-1}.

charge decrease of peak IX during cycling is uncompensated because the charge of peak VIII remains practically constant.

Current peak II is apparently coupled to the cathodic current peak located at more negative potentials, while current peak I is related to the cathodic current peak recorded at more positive potentials (Fig. 3). This indicates that the reaction products formed in the potential range of peak I are electroreduced at more positive potentials than those formed in the potential range of peak II.

For constant $E_{s,a}$ and $E_{s,c}$ values the changes of the E/I profiles during cycling also depend on v (Fig. 3), for instance the charge recorded at 0.006 V s^{-1} is much larger than that obtained at 0.06 V s^{-1}. At low v the negative-going potential sweep exhibits an anodic current in the -0.4 V to -0.75 V range, indicating that the electro-oxidation process proceeds in the same way despite the charge accumulated at the electrode. On the other hand, the stabilized E/I profile recorded at 0.06 V s^{-1} presents a clearer definition of the current peaks than that of the run made at 0.006 V s^{-1}. These effects are more dramatic when $E_{s,a}$ is set at -0.6 V, a value close to that of current peak II (Fig. 4). Then, not only the decrease of the anodic current and the dependence of its rate of decrease with v are observed, but also the establishment of a relatively simple voltammogram involving a Q_a/Q_c ratio equal to

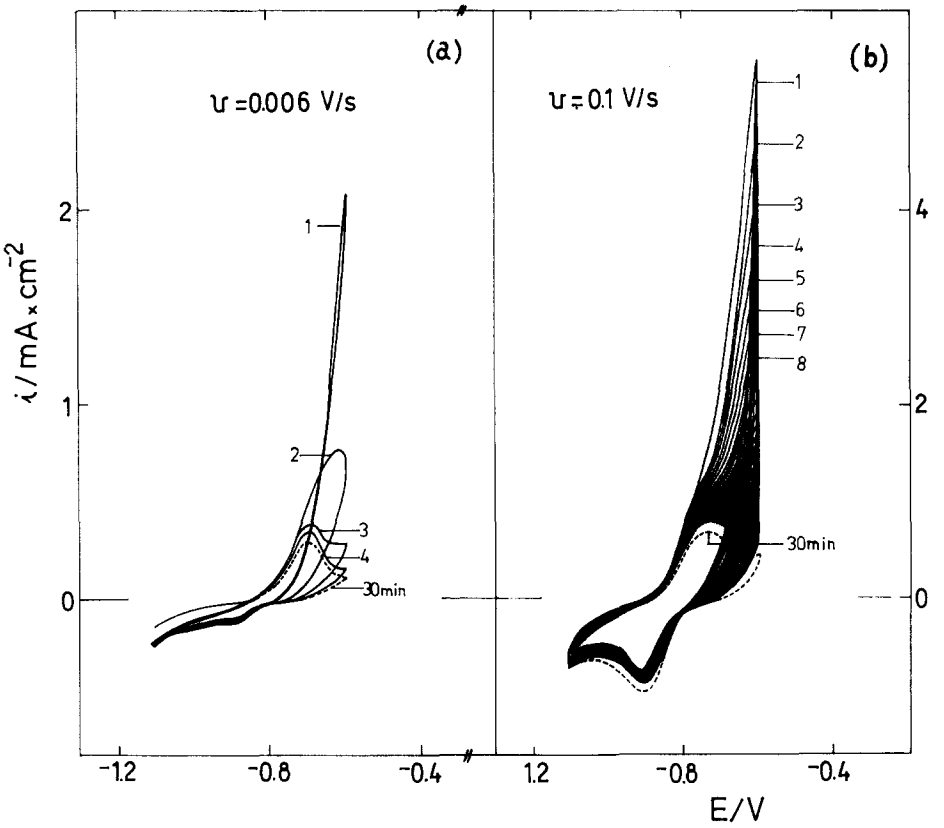

Fig. 4. E/I displays obtained from $E_{s,c} = -1.1$ V to $E_{s,a} = -0.6$ V. (a) $v = 0.006$ V s^{-1}; (b) $v = 0.1$ V s^{-1}.

unity at $v = 0.1$ V s^{-1} (Fig. 4b). This suggests that the electrochemical interface has acquired a different quasi-steady structure. Then, the symmetry of the anodic and cathodic current peaks is nearly the same and the charge playing a part in the overall process is within the order of a few layers of possible oxidation compounds as it is deduced from the Q vs. $1/v$ plots (Fig. 5). The situation described above is only reached whenever $v > 0.03$ V s^{-1}. The new stabilized profile can therefore be analysed in terms of film electroforming–electrostripping processes.

The charge extrapolated at $v \to \infty$ is equal to 0.7 mC cm^{-2}, a value which can be related to that of the $Co(OH)_2$ monolayer if one assumes for the latter the same charge as that of the $Ni(OH)_2$ [22,34,35] monolayer. The separation of the anodic and cathodic current peak potentials ($\Delta E_p = E_{p,I} - E_{p,VIII}$) fits a linear ΔE_p vs. log v relationship (Fig. 6). The slope of the straight line is 0.067 V decade^{-1} and the extrapolation of $\Delta E_p = 0$ corresponds to $v = 0.0001$ V s^{-1}. The fact that at $v < 0.03$ V s^{-1}, $Q_a > Q_c$ can be interpreted in terms of the additional metal electrodissolution contribution, this process being principally associated with current peak II.

The location of the stabilized cathodic current peak depends quite remarkably on

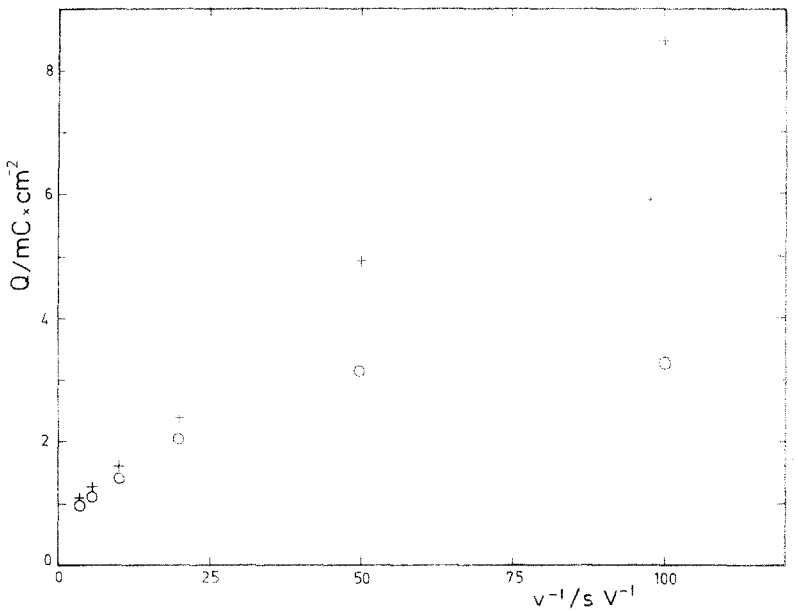

Fig. 5. Potential sweep dependence of the charge involved in the stabilized E/I profiles run between -1.2 V and -0.25 V in solution A. (+) Anodic charge; (○) cathodic charge.

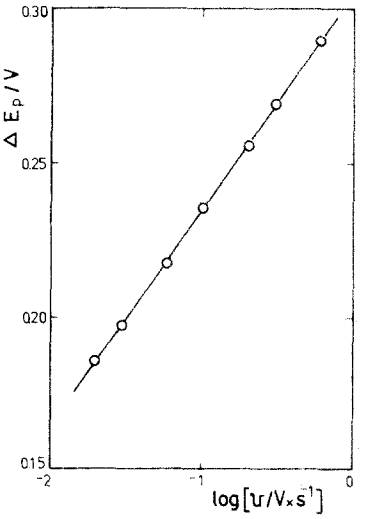

Fig. 6. Dependence of $\Delta E_p = E_{p,I} - E_{p,VIII}$ on υ from the stabilized E/I curves recorded between -1.2 V and -0.5 V in solution A.

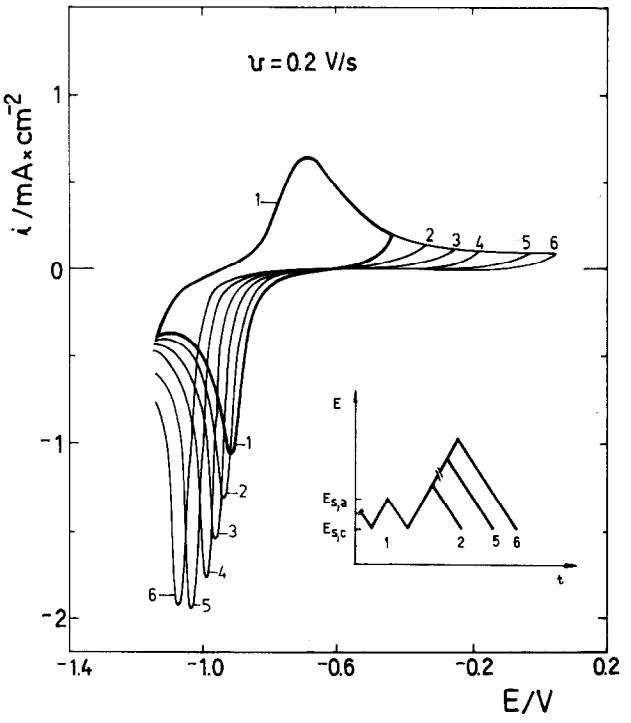

Fig. 7. Influence of the anodic potential limit on the E/I profile recorded with a STPS at 0.2 V s^{-1} in solution A.

$E_{s,a}$, its symmetry changes as the peak height to peak half-width ratio increases as $E_{s,a}$ increases, but its charge is only slightly increased by changing $E_{s,a}$ in the −0.45 V–0.05 V range (Fig. 7). At a constant v, an increase of $E_{s,a}$ is equivalent to an ageing effect of the product formed during the positive-going potential sweep. The ageing appears as an apparent increasing irreversibility of the electroreduction process.

The heights of both peak I and peak VIII increase linearly with v (Fig. 8). This relationship holds for the different electrolytic solutions used in the present work. The potential of peak I remains practically independent of v, but that of current peak VIII decreases linearly with $\log v$, the slope of the straight line being equal to the $2.3(RT/F)$ ratio. This provides an explanation for the slope shown in Fig. 6 which is principally due to the dependence of $E_{p,VIII}$ on v. Nevertheless, the participation of ageing effects associated with the film-forming process can be correlated with the different behaviour of the conjugated current peaks obtained under RTPS. The first TPS E/I display depends more remarkably on v than the following ones, and at low v they exhibit either a possible dissolution of the passivating film or its transformation into a conducting material, since after reaching $E_{s,a}$ the reverse potential sweep shows an anodic current contribution in the potential

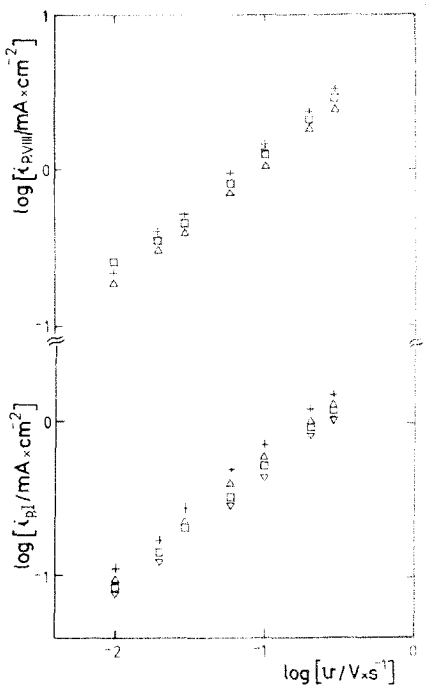

Fig. 8. Dependence of $i_{p,I}$ and $i_{p,VIII}$ on υ resulting from the stabilized E/I displays from $E_{s,c} = -1.2$ V to $E_{s,a} = -0.2$ V. (+) Solution A; (□) solution B; (△) solution C; (▽) solution D.

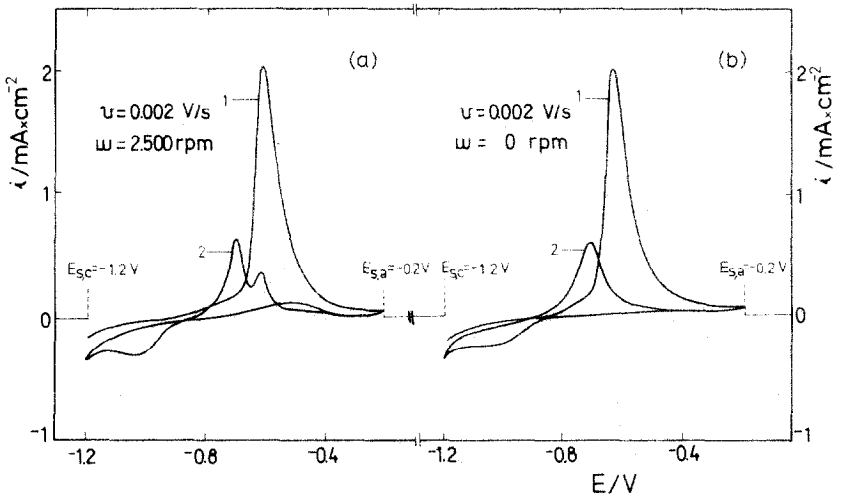

Fig. 9. Influence of ω on the potentiodynamic E/I curves run at $\upsilon = 0.002$ V s^{-1} between -1.2 V and -0.2 V. Solution A. (a) $\omega = 2500$ rpm; (b) $\omega = 0$.

range of peak II. This effect is more pronounced when both $E_{s,a}$ and v decrease.

In the first positive-going potential excursion the height of current peak II approaches a linear dependence with $v^{1/2}$ and the peak potential changes linearly with $\log v$. The slope of the latter is close to $(3/2)(2.3RT/F)$. The corresponding anodic charge during the first sweep changes linearly with v^{-1}, but it furnishes a limiting charge when $v \to 0$.

At $v > 0.05$ V s^{-1}, there is no definite influence of stirring on the voltammograms. Conversely, at very low v, at least for rotation speeds comprised between 250 and 2500 rpm, the second potential sweep run towards the positive potentials shows the apparent splitting of current peak I due to stirring (Fig. 9). However, this effect is related to either a dissolution or a transformation of the product formed in the potential range of current peak II, as the splitting involves a peak whose potential is practically the same as that of current peak II and the preceding negative-going potential sweep exhibits a net anodic current in the -0.4 V to -0.6 V range.

E/I profiles run with combined potential/time perturbations

Once the stabilized E/I profile was attained, the passivated electrode was subjected to a potentiostatic ageing at the potential E_τ, during the time τ (Fig. 10).

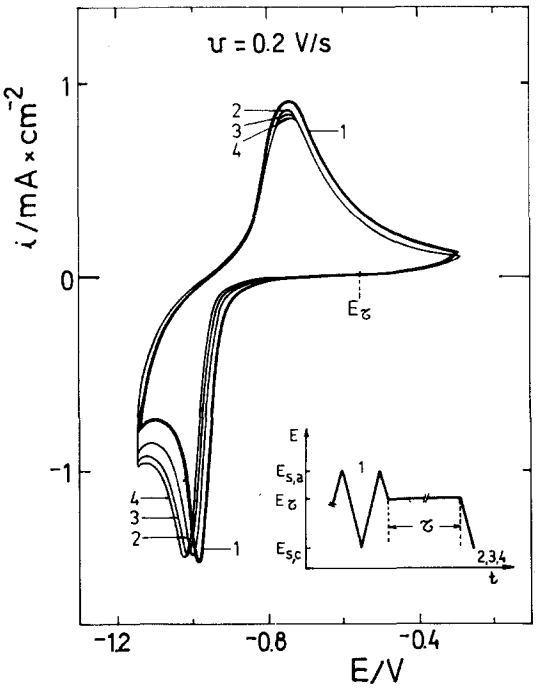

Fig. 10. Potentiodynamic E/I displays obtained with the perturbation program depicted in the figure. Influence of the potentiostatic ageing time τ at $E_\tau = -0.55$ V; $v = 0.2$ V s^{-1}. Solution A. (1) Stabilized E/I profile; (2) $\tau = 1$ min; (3) $\tau = 5$ min; (4) $\tau = 10$ min.

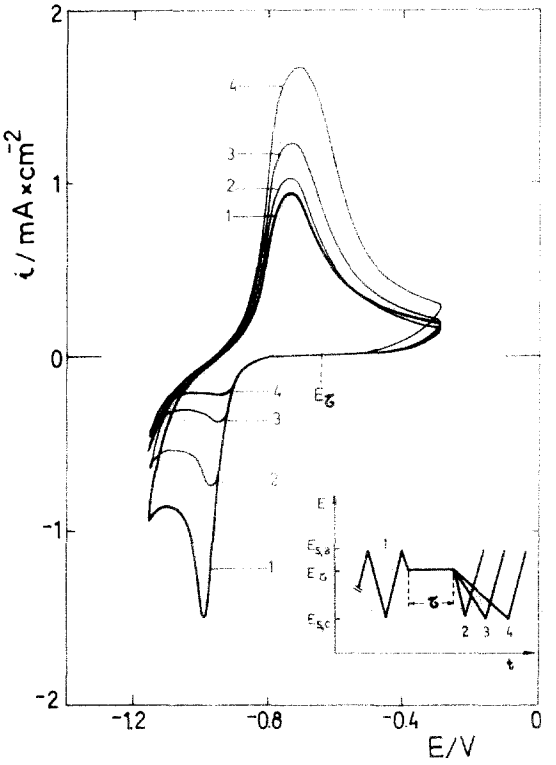

Fig. 11. Potentiodynamic E/I displays obtained with the perturbation program depicted in the figure: $\tau = 3$ min; $E_\tau = -0.65$ V. Solution A. (1) Stabilized RTPS E/I profile at 0.2 V s^{-1}; (2) $v = 0.1$ V s^{-1}; (3) $v = 0.04$ V s^{-1}; (4) $v = 0.02$ V s^{-1}.

The E_τ value was set in the potential range where the current is practically zero during the negative-going potential scan. The charge of current peak VIII at the different τ is nearly constant and the corresponding current peak potential moves towards negative potentials in accordance with τ. This effect is more pronounced the more positive is E_τ.

By running the same type of experiment at constant E_τ and τ (Fig. 11) the electroreduction current peak obtained at different v shows the following interesting features: (1) the peak height increases linearly with v (Fig. 12); (2) the peak potential moves linearly with $\log v$, the slope of this line is $-2.3RT/F$; (3) the initial portions of the E/I electroreduction profile obtained at different v are coincident and obeys a Tafel relationship with the slope -60 mV decade^{-1}. Runs depicted in Fig. 11 show the stepwise increase in Q_a when the v value is decreased stepwise. As already pointed out, this can be ascribed to the partial dissolution of the passivating film occurring at low v.

Comparable results were obtained through the electroreduction of the anodic

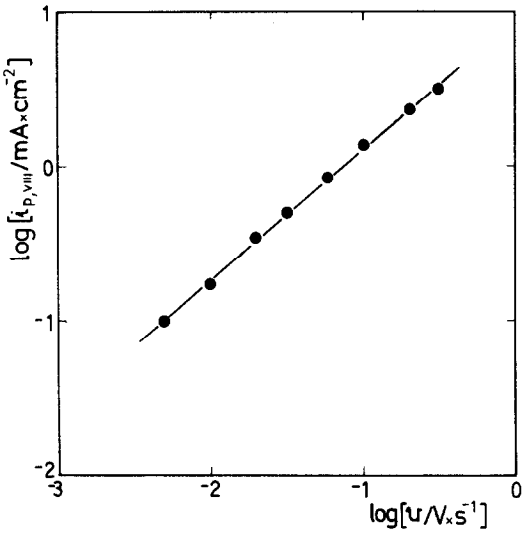

Fig. 12. Dependence of $i_{p,VIII}$ on v after employing the potential perturbation program indicated in Fig. 11; $E_\tau = -0.65$ V. $\tau = 3$ min. Solution A.

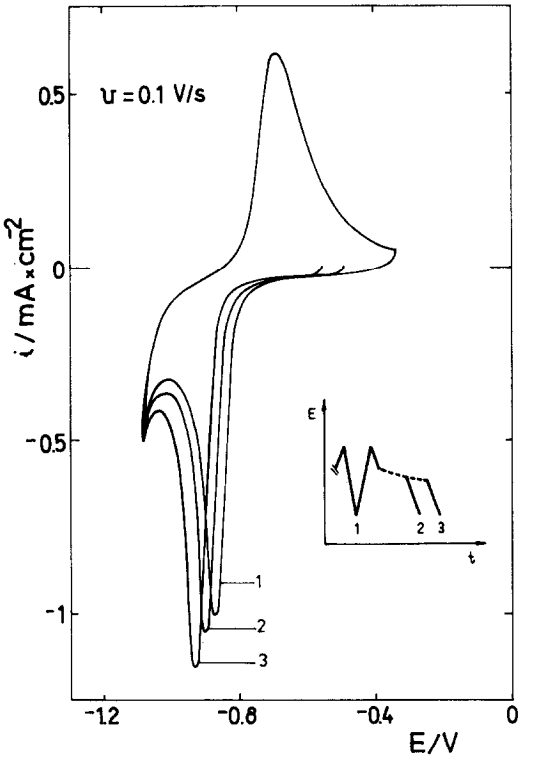

Fig. 13. Potentiodynamic E/I displays obtained with the perturbation program depicted in the figure. Influence of the open-circuit ageing time τ' on the cathodic curves; $v = 0.1$ V s^{-1}. Solution A. (1) Stabilized RTPS E/I profile; (2) $\tau' = 2$ min; (3) $\tau' = 10$ min.

product related to current peak I after the open-circuit ageing at $E_{s,a}$. Then, the electroreduction charge remains constant, but the peak potential shifts towards more negative values the longer the time τ' the electrode remains at open circuit (Fig. 13). The starting potential for the electroreduction process moves towards the negative potential side in accordance with τ'.

Under open-circuit ageing conditions the maximum shift of current peak VIII is reached after approximately 15 min. In the $0 \leqslant \tau' \leqslant 15$ min range, practically no dissolution of the film anodically formed is observed.

Potentiodynamic ageing

When the stabilized profile obtained in the potential range of peaks I and VIII is subjected to the potentiodynamic ageing perturbation program (Fig. 14), a clear splitting of current peak VIII is accomplished.

These runs show the existence of two electroreducible species, namely, one which electroreduces at the potential of current peak VIII, and another which electroreduces at a potential more negative than the former one. The latter is produced by a transformation undergone by the former species during the potentiodynamic ageing. The magnitude of the splitting depends on $E'_{s,c}$, $E_{s,a}$, v and the time τ, the

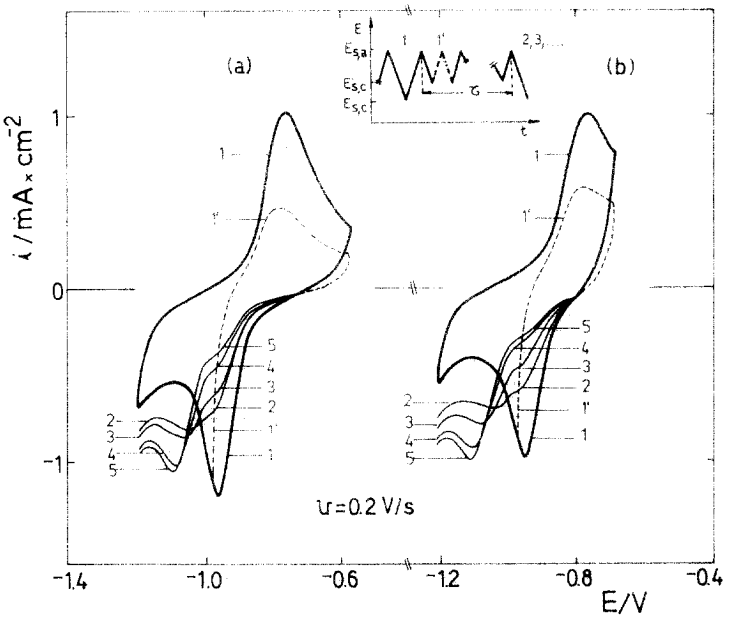

Fig. 14. Potentiodynamic E/I displays obtained with the perturbation program indicated in the figure; $v = 0.2$ V s^{-1}. Solution A. Influence of $E_{s,a}$. $E_{s,a} = -0.57$ V (a); $E_{s,a} = -0.67$ V (b), and the potentiodynamic ageing time τ. (1) Stabilized RTPS E/I profile; (1') first intermediate STPS covering a small potential amplitude; (2) $\tau = 15$ s; (3) $\tau = 30$ s; (4) $\tau = 2$ min; (5) $\tau = 5$ min.

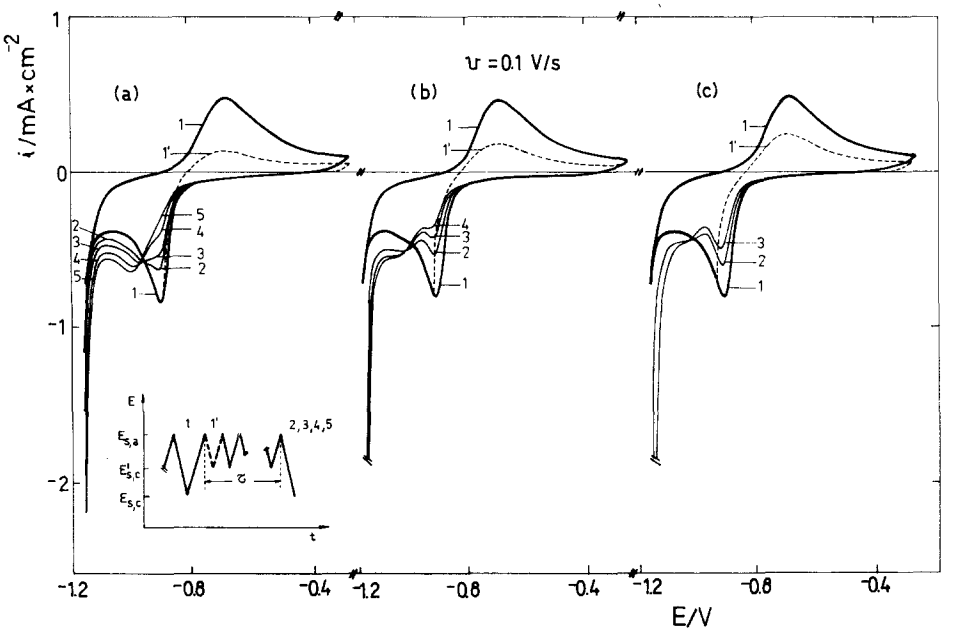

Fig. 15. Potentiodynamic E/I displays obtained with the perturbation program indicated in the figure; $v = 0.1$ V s^{-1}. Solution B. Influence of $E'_{s,c}$ and of the potentiodynamic ageing time. (a) $E'_{s,c} = -0.88$ V; (2) $\tau = 15$ s; (3) $\tau = 30$ s; (4) $\tau = 1$ min; (5) $\tau = 2$ min. (b) $E'_{s,c} = -0.92$ V: (2) $\tau = 1$ min; (3) $\tau = 3$ min; (4) $\tau = 6$ min. (c) $E'_{s,c} = -0.96$ V: (2) $\tau = 1$ min; (3) $\tau = 5$ min.

intermediate perturbation persisting (Fig. 15). As the splitting of the electroreduction profiles involves a constant charge, the effect can also be ascribed to an ageing process associated with the film anodically formed. The cathodic charge (Q_c) of the current peak located at -0.97 V gradually decreases, while simultaneously that of the current peak at -1.1 V increases as the time τ spent in the RTPS between $E'_{s,c}$ and $E_{s,a}$ increases. The maximum splitting is achieved when $E'_{s,c}$ is located in the neighbourhood of the peak VIII potential. The potentials of the split peaks are in good agreement with the potentials of the current peaks identified as peak VIII and peak IX in the RTPS. Therefore, from these results one infers that ageing processes are coupled to the electroformation and electroreduction of the $Co/Co(OH)_2$ electrode.

The same type of potential perturbation program was applied in the negative potential side (Fig. 16). In this case no ageing is observed since the interface is made of the partially clean metal electrode. However, an increase of Q_a and Q_c, and a shift of current peak I towards more positive potentials are noticed after the intermediate RTPS perturbation. These effects can be partially attributed to a probable increase in the electrode roughness promoted by the intermediate RTPS, in good agreement with the charge increase in the electroreduction profile due to the increasing metal active dissolution.

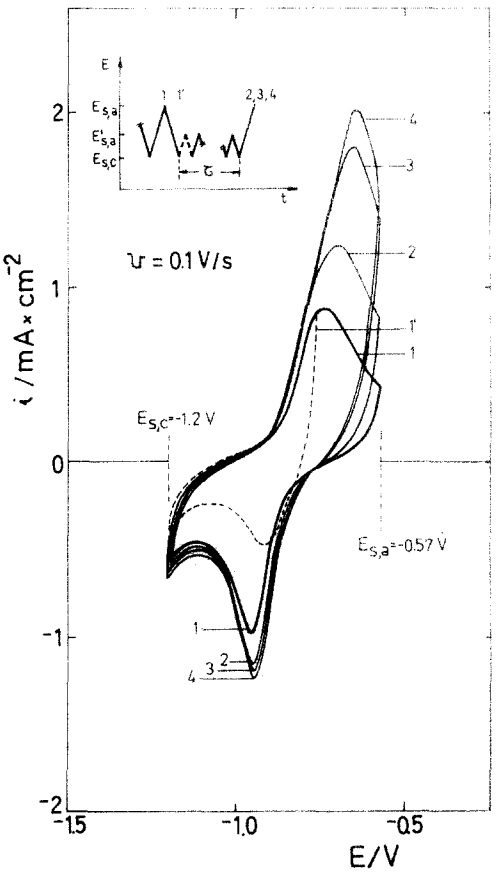

Fig. 16. Potentiodynamic E/I displays obtained with the perturbation program indicated in the figure; $\upsilon = 0.1\ V/s^{-1}$. Solution A. Influence of the potentiodynamic ageing time τ. (1) Stabilized RTPS E/I profile; (2) $\tau = 1$ min; (3) $\tau = 5$ min; (4) $\tau = 10$ min.

DISCUSSION

The cobalt electrode in alkaline solutions already in the potential range where the Co(II) species are thermodynamically stable, shows a passivation effect which is noticed through the gradual change of the potentiodynamic E/I profile during the potential cycling. From this change of the E/I profile it is deduced that cobalt exhibits two completely different electrochemical behaviours, namely, one which is represented by the first potentiodynamic E/I profile and another which corresponds to the E/I profile resulting after a prolonged RTPS. The first behaviour is associated with a large contribution of the metal electrodissolution process which occurs in the potential range of the first complex anodic current peak. The latter contains two distinguishable current contributions. The one at more negative potentials decreases

rapidly during the potential cycling and is accompanied by a decrease of the overall anodic charge, the Q_a/Q_c charge ratio approaching a value equal to unity. The excess of anodic charge during the initial cycling is related to the electrodissolution of the metal.

The second behaviour which corresponds to the stabilized E/I profile obtained after the prolonged potential cycling, involves only the appearance of the anodic current peak I at a potential slightly more negative than the potential of current peak II recorded in the first potential scan. For the second behaviour the corresponding conjugated cathodic current peak is current peak VIII located in a potential range which depends on the anodic switching potential. The stabilized E/I profile is very reproducible, and it involves a Q_a/Q_c ratio equal to unity. This relationship is maintained; meanwhile the switching potential values are in the range of the thermodynamic stability of the Co/Co(II) couple. The gradual change of the E/I profile in the potential range of the hydrogen evolution reaction reveals an increasing polarization effect when the stabilized profile is attained.

The behaviour of cobalt in alkaline solutions in the stability range of Co(II) species, can be explained through the formation of a complex-type electrochemical interface during the potential cycling. The passivation of the cobalt electrode is regarded as due to the formation of an underfilm of CoO next to the metallic surface [21]. This applies to the present results in terms of the primary passivation effect which is the object of this work. As in acid solutions it is evident that a full coverage of the metal surface by adsorbed OH is the minimum requirement to induce the passivity of the metal [21,36]. Taking into account the adsorbability characteristics of OH^- ions, the initial stage of the electrodissolution process should follow the general pattern already discussed for the iron metal electrodes in the alkaline electrolytes [37–39], namely:

$$Co(H_2O)_{ad} + OH^- = Co(OH^-)_{ad} + H_2O \quad (1)$$

$$Co(OH^-)_{ad} = Co(O_{ad} + e \quad (2)$$

$$Co(OH)_{ad} = Co(OH)^+_{ad} + e \quad (3)$$

$$Co(OH)^- + Co(OH^+) = Co(OH)_2 \quad (4)$$

Consecutive reactions (1–4) explain the initial formation of a cobaltous hydroxide layer starting from the electro-oxidation of the base metal surface and also involve earlier mechanisms as limiting cases [11,13]. Ellipsometry shows that in the primary passivation region a weakly absorbing layer is formed [14,40]. However, once the first layer is formed the electrodissolution process should proceed in the presence of the film already formed. This can be accomplished through the following reaction formalism:

$$nCo(OH)_{ad} = Co(OH)_2 + (n-2)Co(OH)_{ad} + Co \quad (5)$$

Reaction (5) implies the formation of an outer $Co(OH)_2$ layer, together with an inner $Co(OH)_{ad}$ monolayer yielding a sandwich-type structure such as those which have already been described for many electrochemical systems involving the formation of

oxo- and oxo-hydroxo-metal-containing species on conducting substrates [27,29,41]. In these sandwich-type structures, the relatively fast proton transfer through the film is to a great extent responsible for the kinetic behaviour of the overall electrochemical interface. In the first plateau, electro-oxidation at constant current has shown the formation of $Co(OH)_2$ on Co, and further oxidation leads to a potential rise which accompanies the formation of a CoO layer between the Co metal and the $Co(OH)_2$ film [16]. The occurrence of reaction (5) should account for the change of the electrochemical behaviour of the electrode from the initial behaviour to that of the stabilized interface once the thickness of the cobaltous hydroxide has acquired a sufficiently large value to slow down the base metal electrodissolution process. When this situation is achieved, the inner part of the complex interface becomes the site of the electrochemical reaction. Then, the electron transfer and the proton transfer processes are coupled. The formalism of this reaction can be written as follows:

$$[Co(OH) \cdot H_2O][Co(OH)_2 \cdot H_2O] = [CoO]_1 + [Co(OH)_2 \cdot 2\,H_2O] + H^+ + e \qquad (6)$$

This reaction should correspond to the response of the stabilized I/E profile. Accordingly, the same charge is involved during the electro-oxidation and electroreduction process, as the process itself can be associated with that of an oxygen monolayer buildup and removal in the inner layer (i) of the sandwich-type electrode during each triangular potential scan. The charge involved in the stabilized I/E profile is precisely of the order of magnitude expected for such a reaction. Hence, the corresponding overall process can be put forward as follows:

$$[Co \cdot Co(OH)_2 \cdot H_2O] + 2\,OH^- = [CoO \cdot Co(OH)_2 \cdot 2\,H_2O] + 2\,e \qquad (7)$$

Reaction (7) is formally equivalent to the oxygen monolayer electroadsorption and electrodesorption at noble metal electrodes which are covered by a metal hydroxide, such as the $Pt/Ni(OH)_2$/alkaline electrolyte electrode [27,29,41]. Many electrochemical interfaces of the metal/oxide metal(1)/oxide metal(2)/electrolyte type have been described. For cobalt, two sandwich-type structures were found, namely $Co/CoO/Co_3O_4$ [13] and $Co/CoO/Co(OH)_2$ [42]. The two metal oxide species can differ in either hydration degree or oxidation state or in both at the same time. These sandwich-type interfaces can be considered under two limiting situations. One corresponds to layer thickness values < 1 nm. In this case the electron transfer by tunnel effect makes the electrochemical behaviour of these interfaces comparable to those observed in the electrosorption of atom monolayers on the conducting substrate. This is the situation which is apparently approached when the stabilized E/I profile is obtained with the cobalt electrode in the alkaline electrolytes. On the other hand, when the film thickness exceeds 2 nm, then the potential distribution in the different layers of the film and their ionic and electronic conductivities become important in defining the electrochemical characteristics of the interface. Thus, for the particular case of the $Co/CoO/Co_3O_4$ interface, Sato and Ohtsuka [17] suggested that the Co_3O_4 layer grows approximately linearly with the applied potential while the thickness of the CoO inner layer seems to depend on the applied potential in a more complex manner. Cations are generally recognized as the most mobile

species in transition metal oxides, and it is possible that the potential drop in the CoO layer becomes independent of the CoO layer thickness and if this potential drop determines the current flow through the film, then the thickness of the CoO should approach a constant value.

If the processes associated with the stabilized I/E profile were related to a reaction at the outer layer of the sandwich-type structure one should expect the same behaviour to be encountered with a platinum electrode covered by a cobaltous hydroxide film. However, such behaviour was certainly not observed [43].

The electrochemical characteristics of the sandwich-type cobaltous hydroxide electrode is sensitive to the ionic composition of the system. The largest cobaltous hydroxide film thickness deduced from the charge value is of the order of 2 nm. The kinetic behaviour of these films is similar to that already reported for nickelous hydroxide films, namely, both depend on their degree of hydration and on the extent of ions either occluded in the films or adsorbed on them. These characteristics derive from the colloidal nature of the film which is demonstrated through the response of cobaltous hydroxide electrodes produced by colloidal precipitation on different conducting substrates [43].

The similarity of the stabilized E/I profile of the cobalt/cobalt hydroxide interface with those concerning the oxygen electroadsorption and electrodesorption on noble metal is also reflected through the appearance of ageing processes. The latter manifests through the gradual and systematic shift of the electroreduction current peak (peak VIII) when the potential perturbation allows us to control the lifetime of the oxidized species. Thus, under both open-circuit ageing (Fig. 13) and potentiostatic ageing conditions (Figs. 10, 11), the electroreduction current peak potential becomes more negative as the corresponding ageing time increases. Likewise, when the ageing is promoted by the potentiodynamic perturbation the splitting of the electroreduction current peak is observed (Figs. 14, 15) which makes clear the existence of at least two reactants entering the electroreduction process. The overall electroreduction charge is, however, independent of the relative amount of those reactants, a fact which indicates that the corresponding species probably involve the same oxidation state but a different structural configuration. Through ageing, the most stable O-containing species is promoted in the same way already described for other O-containing layers and oxo-hydroxide-containing thin multilayers [26,28,30,44–46]. Therefore, in the present case the ageing effect should be related to a kind of chemical reaction proceeding in the hydrated cobaltous oxide film, probably involving a reaccommodation of the oxygen atoms through a place exchange mechanism [47]. Then, the overall electroreduction reaction involved in eqn. (5) has to be put forward in terms of the following reaction pattern:

$$\begin{array}{l} [CoO]_u \cdot n\,H_2O \\ \quad\Big\downarrow k \qquad \overset{+2\,H^+ + 2\,e}{\searrow\!\!\rightarrow} \\ [CoO]_s \cdot n'\,H_2O \qquad \underset{+2\,H^+ + 2\,e}{\nearrow\!\!\rightarrow} \end{array} \quad Co \cdot Co(OH)_2 \cdot H_2O \qquad (8)$$

where u and s denote the unstable and the stable CoO configuration and k is the rate constant of the ageing process of the oxidized surface species. Analogously, the electro-oxidation process is related to the same reaction pattern as follows:

$$\mathrm{Co \cdot Co(OH)_2 \cdot H_2O} \begin{array}{l} \xrightarrow{e,\,H^+} [\mathrm{CoO}]_u \cdot n\,\mathrm{H_2O} \\ \qquad\qquad \downarrow \\ \xrightarrow{e,\,H^+} [\mathrm{CoO}]_s \cdot n'\,\mathrm{H_2O} \end{array} \qquad (9)$$

The electro-oxidation reaction involves a single species, since the inner layer actually corresponds to the first plane of bare cobalt atoms, so that no ageing of reactants should be expected for the electro-oxidation processes.

Following the same procedure already described for nickelous hydroxide electrodes [26,28], the rate constant of the ageing process, namely that of the chemical conversion of the u-species into the s-species, is estimated from the runs under potentiodynamic ageing conditions, after considering that the overall charge which participates in the ageing process is equal to the total anodic charge. This is accomplished by fixing the experimental conditions in such a way that the splitting of the electroreduction profile comprises a constant charge overall value. Then, on the basis of a first-order kinetics for the ageing process, the estimated value of k, at 25°C, is 8×10^{-2} min^{-1}. This figure is of the same order of magnitude as that of the ageing of nickel oxo-hydroxo-species in the same electrolyte solution.

The kinetic parameters derived from the stabilized E/I profiles fit linear i vs. υ and E_p vs. log υ relationships. These relationships are expected for an electrochemical reaction involving a film build up and removal on the electrode under an electron-transfer rate control [48–50]. The simplest mechanism which accounts for those kinetic relationships, in terms of reaction patterns (8) and (9), can be given in terms of two consecutive steps:

$$\mathrm{Co\big[Co(OH)_2 \cdot x\,H_2O\big] \rightarrow CoOH\big[Co(OH)_2 \cdot (x-1)H_2O\big] + H^+ + e} \qquad (10)$$

$$\mathrm{CoOH\big[Co(OH)_2 \cdot (x-1)H_2O\big] \rightarrow CoO\big[Co(OH)_2 \cdot (x-1)H_2O\big] + H^+ + e} \qquad (11)$$

where reaction (11) should be seen as the rate-determining reaction. Reaction (10), which is the initial stage in the electro-oxidation of most metals in aqueous electrolytes, is a relatively fast reaction [51], and is also formally related to the reversible initial stage of oxygen electrosorption on noble metal electrodes. The apparent independence of the kinetic parameters derived from the potentiodynamic data on the solution pH is also explained by the fact that at the inner layer of the sandwich-type electrode the pH is principally determined by the hydrolysis equilibria of the precipitated hydrated cobalt oxo-hydroxides.

CONCLUSIONS

The potentiodynamic response of Co in alkaline solutions exhibits two limiting electrochemical behaviours. During the initial potential cycling the main anodic

contribution is the electrodissolution of the base metal, while after a prolonged potential cycling the electrochemical interface acquires a sandwich-type structure coinciding with the structures recently described by various authors on different metals [27,52–54]. The present results reveal the occurrence of ageing process related to the reaction product formed in the first oxidation stage of cobalt in the alkaline electrolyte. These species can be considered as passivity precursors. From the phenomenological standpoint the cobalt electrode in alkaline solutions behaves in a similar way to other transition metals in the same type of electrolytes [26–30,43–47].

ACKNOWLEDGEMENT

INIFTA is sponsored by the Consejo Nacional de Investigaciones Científicas y Técnicas, the Universidad Nacional de La Plata and the Comisión de Investigaciones Científicas (Provincia de Buenos Aires). This work is partially supported by the Regional Program for Scientific and Technological Development of the Organization of American States. One of us (H.G.M.) thanks the University of Valparaíso for leave of absence.

REFERENCES

1 N. Maki and N. Tanaka in A.J. Bard (Ed.), Encyclopedia of Electrochemistry of the Elements Vol. III, Marcel Dekker, New York, 1975, p.43.
2 G.W.F. Briggs, Specialist Periodical Reports on Electrochemistry, Vol. 4, The Chemical Society, London, 1974, p. 43.
3 S.V. Falk and A.J. Salkind, Alkaline Storage Batteries, Wiley, New York, 1966.
4 D.F. Pickett and J.T. Maloy, J. Electrochem. Soc., 125 (1978) 1026.
5 B.N. Efremov, M.R. Tarasevich, G.I. Zakharkin and S.R. Zhukov, Elektrokimiya, 14 (1978) 1504; Zh. Fiz. Khim., 52 (1978) 1671.
6 G. Grube and O. Feucht, Z. Elektrochem., 28 (1922) 568.
7 S.E.S. El Wakkad and A. Hickling, Trans. Faraday Soc., 46 (1950) 820.
8 E. Deltombe and M. Pourbaix, Proc. 6th C.I.T.C.E. Meeting, Butterworths, London, 1965, p. 153.
9 H. Göhr, Electrochim. Acta, 11 (1966) 827.
10 P. Benson, G.W.D. Briggs and W.F.K. Wynne-Jones, Electrochim. Acta, 11 (1966) 1079.
11 R.D. Cowling and A.C. Riddiford, Electrochim. Acta, 14 (1969) 981.
12 T. Ohtsuka and N. Sato, J. Jap. Inst. Met., 39 (1975) 60.
13 T. Ohtsuka and N. Sato, Boshoku Gijutsu, 24 (1975) 289.
14 T. Ohtsuka, K. Kudo and N. Sato, J. Jap. Inst. Met., 40 (1976) 124.
15 T. Ohtsuka and N. Sato, 27th I.S.E. Meeting. Ext. Abs. No. 105, Zurich, 1976.
16 K. Kudo, N. Sato and T. Ohtsuka in R.P. Frankenthal and J. Kruger (Eds.) Passivity of Metals, The Electrochemical Society, Princeton, 1978, p. 918.
17 N. Sato and T. Ohtsuka, J. Electrochem. Soc., 125 (1978) 1735.
18 G.W. Simmons, E. Kellerman and H. Leidheiser, J. Electrochem. Soc., 123 (1976) 1276.
19 G.W. Simmons in R.P. Frankenthal and J. Kruger, (Eds.), Passivity of Metals, The Electrochemical Society, Princeton, 1978, p. 889.
20 A. Vertes, I. Nagyn, M. Varsanyi, L. Kiss, L. Mag and H. Leidheiser, Kem. Kozl., 53 (1980) 249.
21 W.K. Behl and J.E. Toni, J. Electroanal. Chem., 31 (1971) 63.
22 T.R. Jayaraman, V.K. Venkatesan and H.V.K. Udupa, Electrochim. Acta, 20 (1975) 209.
23 L.D. Burke and O.J. Murphy, J. Electroanal. Chem., 109 (1980) 373.
24 L.D. Burke and O.J. Murphy, J. Electroanal. Chem., 112 (1980) 379.

25 A. Dechenaud, C. Guillet, I. Barralis and J. Ledion, Metaux, 631 (1978) 71.
26 R.S. Schrebler Guzmán, J.R. Vilche and A.J. Arvia, J. Appl. Electrochem., 9 (1979) 183.
27 M.E. Folquer, J.R. Vilche and A.J. Arvia, J. Electrochem. Soc., 127 (1980) 2634.
28 H. Gomez Meier, J.R. Vilche and A.J. Arvia, J. Appl. Electrochem., 10 (1980) 611.
29 V.C. Macagno, J.R. Vilche and A.J. Arvia, J. Electrochem. Soc., in press.
30 M. Lopez Teijelo, J.R. Vilche and A.J. Arvia, J. Electroanal. Chem., 131 (1982) 331.
31 J.R. Vilche and A.J. Arvia, Corros. Sci., 15 (1975) 419.
32 J.R. Vilche and A.J. Arvia, J. Electrochem. Soc., 123 (1976) 1061.
33 J.R. Vilche and A.J. Arvia, Corros. Sci., 18 (1978) 441.
34 J.L. Weininger and M.W. Breiter, J. Electrochem. Soc., 110 (1963) 484.
35 R.N. O'Brien and K.V.N. Rao, J. Electrochem. Soc., 112 (1965) 1245.
36 K.E. Heusler, Corros. Sci., 6 (1966) 183.
37 J.R. Vilche and A.J. Arvia, Proc. 7th Int. Congr. Met. Corros., Rio de Janeiro, 1978, p. 245.
38 R.S. Schrebler Guzmán, J.R. Vilche and A.J. Arvia, Electrochim. Acta, 24 (1979) 395.
39 J.O. Zerbino, J.R. Vilche and A.J. Arvia, J. Appl. Electrochem., 11 (1981) 703.
40 W. Paik and J.O'M. Bockris, Surf. Sci., 28 (1971) 61.
41 R.E. Carbonio, V.C. Macagno, M.C. Giordano, J.R. Vilche and A.J. Arvia, J. Electrochem. Soc., in press.
42 T. Ohtsuka, Ph.D. Thesis, Hokkaido University, 1976.
43 H. Gomez Meier, Ph.D. Thesis, La Plata University, 1980.
44 R.S. Schrebler Guzmán, J.R. Vilche and A.J. Arvia, J. Electrochem. Soc., 125 (1978) 1578.
45 J.R. Vilche and A.J. Arvia, Lat. Am. J. Chem. Eng. Appl. Chem., 9 (1979) 35.
46 R.S. Schrebler Guzmán, J.R. Vilche and A.J. Arvia, J. Appl. Electrochem. 11 (1981) 551.
47 A.J. Arvia, Isr. J. Chem., 18 (1979) 89.
48 S. Srinivasan and E. Gileadi, Electrochim. Acta, 11 (1966) 321.
49 E. Laviron, J. Electroanal. Chem., 52 (1974) 355, 395.
50 H. Angerstein-Kozlowska, J. Klinger and B.E. Conway, J. Electroanal. Chem., 75 (1977) 45.
51 J.R. Vilche and A.J. Arvia, Anal. Acad. Cs. Exac. Fis. Nat., Buenos Aires, 33 (1981) 33.
52 M. Sakashita and N. Sato, Corrosion, 35 (1979) 351.
53 M.M. Lohrengel, P.K. Richter and J.W. Schultze, Ber. Bunsenges. Phys. Chem., 83 (1979) 490.
54 J.O. Zerbino and A.J. Arvia, J. Electrochem. Soc., 126 (1979) 93.